Diabetes in Mice With Selective Impairment of Insulin Action in Glut4-Expressing Tissues

Hua V. Lin,[1] Hongxia Ren,[1] Varman T. Samuel,[2] Hui-Young Lee,[2] Taylor Y. Lu,[1] Gerald I. Shulman,[2] and Domenico Accili[1]

OBJECTIVE—Impaired insulin-dependent glucose disposal in muscle and fat is a harbinger of type 2 diabetes, but murine models of selective insulin resistance at these two sites are conspicuous by their failure to cause hyperglycemia. A defining feature of muscle and fat vis-à-vis insulin signaling is that they both express the insulin-sensitive glucose transporter Glut4. We hypothesized that diabetes is the result of impaired insulin signaling in all Glut4-expressing tissues.

RESEARCH DESIGN AND METHODS—To test the hypothesis, we generated mice lacking insulin receptors at these sites ("GIRKO" mice), including muscle, fat, and a subset of Glut4-positive neurons scattered throughout the central nervous system.

RESULTS—GIRKO mice develop diabetes with high frequency because of reduced glucose uptake in peripheral organs, excessive hepatic glucose production, and β-cell failure.

CONCLUSIONS—The conceptual advance of the present findings lies in the identification of a tissue constellation that melds cell-autonomous mechanisms of insulin resistance (in muscle/fat) with cell-nonautonomous mechanisms (in liver and β-cell) to cause overt diabetes. The data are consistent with the identification of Glut4 neurons as a distinct neuroanatomic entity with a likely metabolic role. ***Diabetes*** **60:700–709, 2011**

Type 2 diabetes (T2D) can be viewed as a failure of homeostatic mechanisms that promote nutrient turnover and storage in response to hormonal cues. Although the factors that favor disease progression are heterogeneous, evidence from prospective human studies indicates that impairment of insulin-dependent glucose uptake and utilization is an early event in disease pathogenesis (1). The largest fraction of insulin-dependent glucose disposal (~70%) occurs in skeletal muscle and is mediated by the insulin-responsive glucose transporter Glut4 (2). A quantitatively smaller contribution (5–20%) is provided by adipose tissue (3). That skeletal muscle is an important site of insulin resistance in humans and that impaired insulin action in muscle leads to adaptive changes in nutrient use from carbohydrates to lipids and to compensatory β-cell hyperplasia are beyond dispute (4). Similarly, insulin resistance in adipose tissue is contributory to the pathogenesis of diabetes not only through impaired glucose disposal but also through excess lipolysis and adipokine/cytokine production (5). But models of muscle/fat insulin resistance, such as those generated by targeted inactivation of insulin receptor (InsR) (6–8) or the insulin-responsive glucose transporter Glut4 (9) in those tissues, have limited metabolic consequences and do not result in overt diabetes. One possible explanation is that an independent "hit" on the pancreatic β-cell is required, leading to reduced insulin secretion or curtailing β-cell hyperplasia in response to insulin resistance (10,11). Alternatively, these data can be construed to suggest that the transition from compensated insulin resistance to overt diabetes requires impairment of insulin action at additional sites (12).

Insulin signaling in the central nervous system (CNS) affects systemic insulin sensitivity and glucose metabolism (13–16). It is intriguing that Glut4 is also expressed in discrete brain regions, where its levels are increased in murine models of T2D and decreased in streptozotocin-induced diabetes (17–20). The contribution of CNS Glut4 to insulin action and glucose homeostasis remains unclear, because Glut4-positive cells express additional glucose transporters (e.g., Glut3) whose contribution to overall glucose uptake likely dwarfs that of Glut4 (21). Also, the brain as a whole metabolizes glucose in an insulin-independent manner (22).

In addition to the important role of Glut4 in insulin-dependent glucose uptake, its expression in tissues that do not require insulin for glucose uptake (e.g., CNS) might represent a vestigial marker of tissue insulin responsiveness independently of the actual role of Glut4 proper in glucose uptake, and a generalized impairment of insulin action in all Glut4 tissues might underlie the pathogenesis of diabetes. Accordingly, we set out to generate a murine model of impaired insulin signaling in Glut4-expressing tissues. In doing so, the driving hypothesis was that the cause for the absence of diabetes in murine models of muscle/fat insulin resistance is the preservation of insulin signaling in other insulin-sensitive tissues (as characterized by Glut4 expression), and primarily in Glut4 neurons of the CNS. To test this hypothesis, we engendered insulin resistance in Glut4-expressing tissues by targeted inactivation of InsR and performed metabolic analyses of the resulting phenotypes.

RESEARCH DESIGN AND METHODS

DNA constructs and experimental animals. A DNA construct encoding *GLUT4-Cre* was engineered by cloning a 2.4-kb human *GLUT4* promoter fragment (23) into pSP73 vector, containing Cre cDNA preceded by a β-globin intron. The purified linearized DNA fragment was microinjected into fertilized eggs from *C57BL*/6 × *FVB* mice. We obtained two founders (535 and 546) that

From the [1]Department of Medicine, Columbia University, New York, New York; and the [2]Department of Medicine, Yale University School of Medicine, New Haven, Connecticut.
Corresponding author: Domenico Accili, da230@columbia.edu.
Received 27 July 2010 and accepted 3 December 2010.
DOI: 10.2337/db10-1056
This article contains Supplementary Data online at http://diabetes.diabetesjournals.org/lookup/suppl/doi:10.2337/db10-1056/-/DC1.
H.V.L. and H.R. contributed equally to this work.
H.V.L. is currently affiliated with Merck Research Laboratories, Rahway, New Jersey.

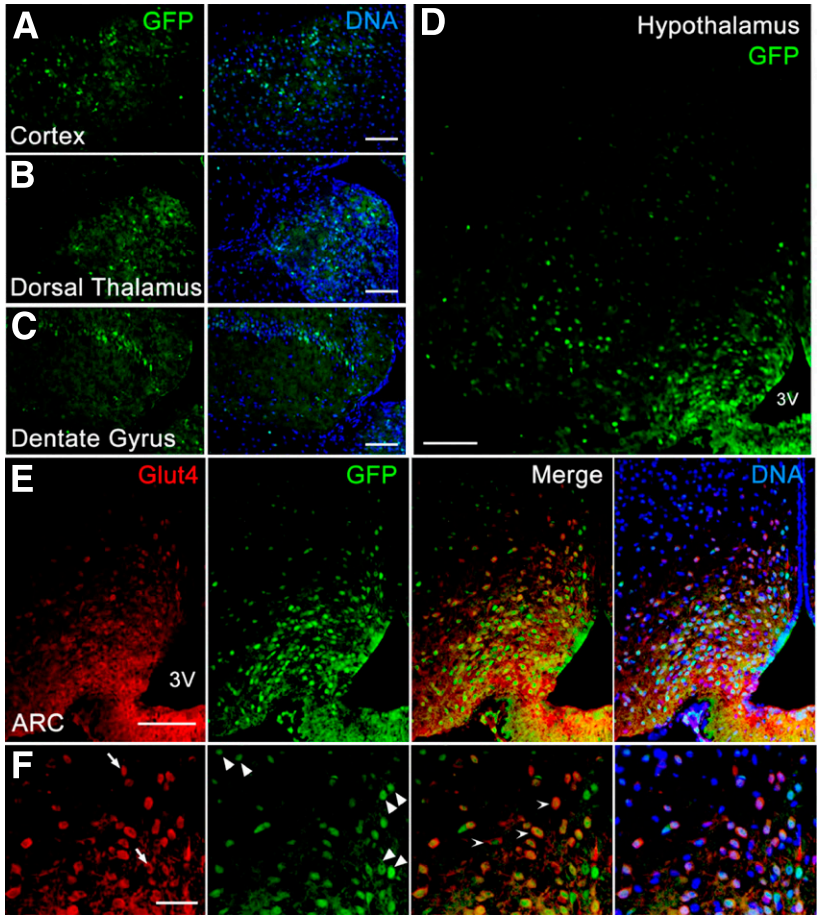

FIG. 1. *GLUT4-Cre*–mediated recombination in the brain and Glut4 neurohistochemistry. *A–D*: GFP immunoreactivity (green) and Hoechst nuclear staining (blue) in cortex (*A*), thalamus (*B*), dentate gyrus (*C*), and hypothalamus (*D*) of *GLUT4-Cre/Rosa26-Gfp* mice. *E*, *F*: Immunostaining with anti-Glut4 (red) and anti-GFP (green) antibodies in mediobasal hypothalamus of *GLUT4-Cre/Rosa26-Gfp* mice; *F* is a higher magnification view of *E*, with arrows indicating Glut4-positive/GFP-negative cell bodies (*left* panel), arrowheads indicating GFP-positive/Glut4-negative cell bodies (second panel from the *left*), and concave arrowheads indicating Glut4-positive/GFP-positive cell bodies (third panel from the *left*). The DNA-counterstained merged image is shown on the *right*. 3V, third ventricle; ARC, arcuate nucleus. Scale bars: 100 μm (*A–E*) and 50 μm (*F*). (A high-quality digital representation of this figure is available in the online issue.)

were characterized for transgene transmission and recombination. The transgene showed autosomal transmission in line 546 and X-linked transmission in line 535. Both lines underwent germ line recombination when transmitted through the dam, but not when transmitted through the sire. When transmitted through the sire, both transgenes were liable to stochastic embryonic activation, leading to generation of animals with varying degrees of chimerism. An example is shown in Supplementary Fig. 1, demonstrating chimeric recombination in liver of GIRKO mice. These events were monitored by genotyping of tail DNA, and chimeric mice were excluded from further analyses. When mice were killed, extensive genotyping was performed to ascertain that mice had undergone recombination only in bona fide Glut4-expressing tissues.

Line 546 transgenics were intercrossed with $Insr^{flox/flox}$ mice (7), and the resulting progeny was intercrossed to yield $Insr^{flox/flox}$ controls and $Insr^{flox/flox,\ GLUT4\text{-}cre}$ (GIRKO) mice that were used for all subsequent phenotypic analyses. Animals were maintained on a mixed background derived from 129/Sv, C57BL/6, and FVB. *GLUT4-Cre* was genotyped using primers 5′-TGGGTCCCATCGGGCCCTTAATT-3′ and 5′-TGGCGATCCCTGAACATGTCCAT-3′, amplifying a 350-bp product in the presence of the transgene. *Rosa26/Gfp* and *Rosa26/Rfp* mice were obtained from Jackson Laboratories. The Columbia University Institutional Animal Care and Utilization Committee and the Yale University Animal Care and Use Committee approved all animal procedures.

Metabolic analyses. Blood glucose was measured by the One-Touch Ultra meter (LifeScan Inc., Milpitas, CA). Insulin and leptin were measured by enzyme-linked immunosorbent assay, and glucagon was measured by radioimmunoassay (Linco Research Inc., St. Charles, MO). Plasma free fatty acids (FFA) and cholesterol were measured by NEFA-HR and Cholesterol-E test reagents (Wako Chemicals, Richmond, VA). Triglycerides were measured by serum triglyceride determination kit (Sigma-Aldrich, St. Louis, MO). β-Hydroxyl butyrate was measured by a colorimetric assay (Pointe Scientific, Canton, MI). Measurements of hepatic glycogen and triglycerides were performed as previously described (24). Body composition was determined using Bruker Minispec NMR (Bruker Optics, Billerica, MA) (16).

In vivo analysis of insulin signaling. Male mice, 12 to 14 weeks old, were fasted overnight, anesthetized, and injected with saline or insulin (5U) into the inferior vena cava. Three minutes after injection, muscle, adipose, liver, heart, and brain tissues were rapidly removed and flash-frozen in liquid nitrogen (25). Detergent extracts were prepared in buffer containing 20 mmol/L Tris (pH 7.6), 150 mmol/L NaCl, 1 mmol/L dithiothreitol, 10 mmol/L EGTA, 1% NP40, 2.5 mmol/L $Na_4P_2O_7$, 1 mmol/L $NaVO_3$, 1 mmol/L β-glycerophosphate, and protease inhibitor cocktail (Roche, Indianapolis, IN). Protein concentration of extracts was determined by bicinchoninic acid assay (Pierce, Rockford, IL). Equal amounts of protein (50–100 μg) were resolved on SDS-PAGE and transferred onto nitrocellulose membranes (Schleicher & Schuell, Keene, NH). Membranes were probed with antibodies against phospho-Akt (Ser473), total Akt (Cell Signaling, Danvers, MA), InsRβ, and β-actin (Santa Cruz Biotechnology, Santa Cruz, CA).

Euglycemic-hyperinsulinemic clamps. Thirteen- to fifteen-week-old normoglycemic male GIRKO mice (n = 10) and control littermates (n = 9) were studied. Euglycemic-hyperinsulinemic clamps were performed in conscious, minimally stressed mice at the Yale Mouse Metabolic Phenotyping Center (http://mouse.yale.edu). Briefly, after anesthesia, an indwelling catheter was placed into the right internal jugular vein. Studies were carried out 4 to 5 days after surgery in overnight fasted mice. Tail tethered using tape and basal glucose turnover were measured using a primed-continuous infusion of [3-^{3}H] glucose for 2 h before the start of clamp. At the start of the clamp, mice received a primed constant infusion of human insulin (15 pmol/kg/min) and continued to receive [3-^{3}H]glucose (0.1 mCi/min, PerkinElmer, Waltham, MA)

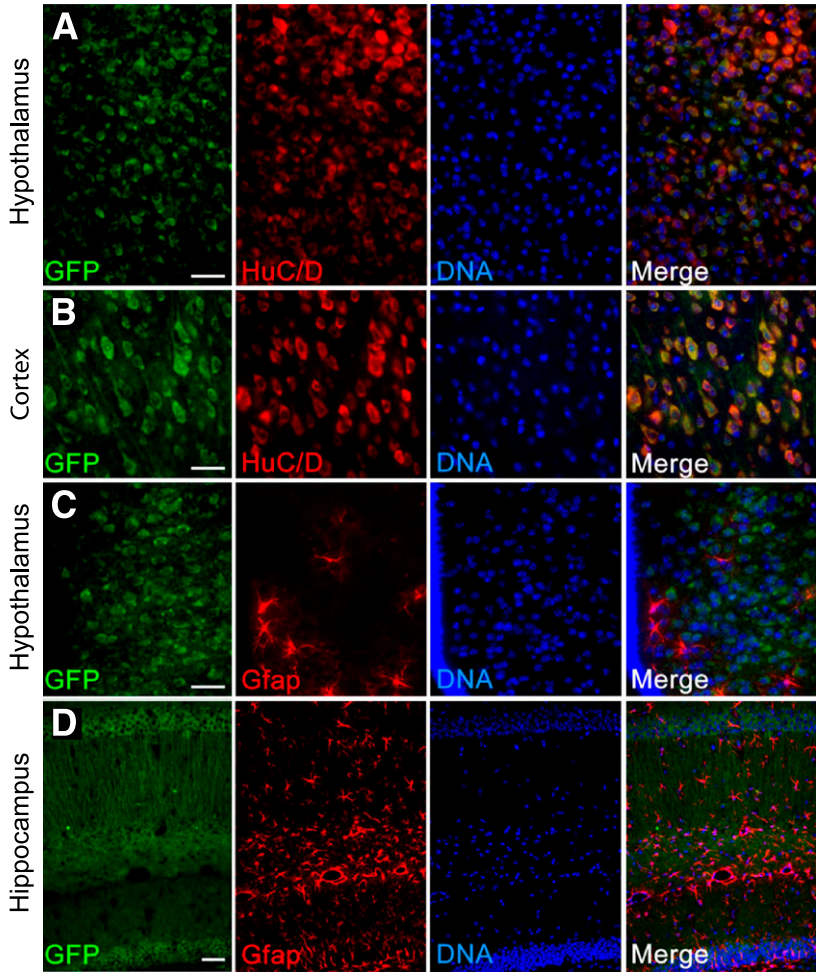

FIG. 2. Colocalization of *GLUT4-Cre*–mediated recombination with neuronal and glial markers. *A*, *B*: Coimmunostaining with GFP (green) and neuronal marker HuC/D (red) antibodies in hypothalamus and cortex of *GLUT4-Cre/Rosa26-Gfp* mice. *C*, *D*: Coimmunostaining with GFP (green) and glial marker Gfap (red) antibodies in hypothalamus and hippocampus of *GLUT4-Cre/Rosa26-Gfp* mice. Scale bars: 50 μm. (A high-quality digital representation of this figure is available in the online issue.)

for the duration of the clamp. Blood samples were collected from tail. Blood glucose was determined at 10- to 20-min intervals. Glucose (20% solution) was infused at a variable rate as required to maintain euglycemia. 2-Deoxy-D-[1-^{14}C]glucose (2-[^{14}C]DG) was administered as a bolus (10 μCi) 75 min after the start of the clamp. Blood samples (20 μL) were taken at −5, 80, 85, 90, 100, 110, and 120 min of clamp for the measurement of plasma [^{3}H] glucose, tritiated water, or 2-[^{14}C]DG concentrations. Additional blood samples (20 μL) were collected before and at the end of clamp for the measurement of plasma insulin and FFA. At the end of the clamp, mice were killed, and liver, gastrocnemius, epididymal fat, and cerebral cortex were flash-frozen in liquid nitrogen. Tissue samples were stored at –80°C for analysis (16).

Indirect calorimetry. Mice were individually housed in a TSE LabMaster system (TSE Systems Inc., Chesterfield, MO) and acclimated to the respiratory chambers for 24–36 h before measurements were taken. Data on gas exchanges, locomotor activity, and food intake were collected every 14 min for 4–5 days (26).

Histology and immunohistochemistry. Adipose tissue and liver were fixed in 10% formaldehyde for hematoxylin–eosin and periodic acid-Schiff staining. Frozen liver embedded in OCT was used for Oil red O staining. Pancreata from 12-week-old male mice were fixed in 10% formaldehyde overnight and embedded in paraffin; consecutive sections 5 μm in thickness were mounted on slides. Sections were stained with antibodies against insulin, glucagon (Sigma-Aldrich San Antonio, TX), Pdx1 (27), and Glut2 (Alpha Diagnostics, Owings Mills, MD) (28).

Statistical methods. All data represent means ± SEM. Datasets were analyzed for statistical significance with one-way ANOVA followed by post hoc Bonferroni test using SPSS software (SPSS Inc., Chicago, IL).

RESULTS

Generation of *GLUT4-Cre* mice. We generated transgenic mice expressing *Cre* off a 2.4-kb *GLUT4* promoter fragment that has been shown to confer tissue-specific expression of a reporter construct (23). We characterized recombination patterns in two *GLUT4-Cre* founders (lines 535 and 546) by crossing them with either *ROSA26-Gfp* or *ROSA26-Rfp* transgenics. Line 546 faithfully recapitulated *Glut4* expression, yielding recombination in skeletal muscle, epididymal and subcutaneous white adipose tissue (WAT) and brown adipose tissue (BAT), heart, and kidney (glomeruli and loop of Henle). We also detected recombination at sites of Glut4 expression heretofore unrecognized, such as ovarian corpora lutea, myometrium, nuclear layers of the retina, and acinar cells in the exocrine pancreas and salivary gland (Supplementary Fig. 1*A* and *B*). Line 535 showed more limited recombination in skeletal muscle and brain (not shown).

In view of literature on Glut4 expression in the CNS (17, 20,21,29,30), we analyzed patterns of *GLUT4-Cre*–mediated recombination in this organ using *GLUT4-Cre* × *Rosa26-Gfp* mice. Green fluorescent protein (GFP) immunohistochemistry in brain sections of the resulting progeny revealed Cre-mediated recombination in scattered subsets of cells

throughout the CNS, including cortical pyramidal neurons, cerebellar Purkinje-like cells, olfactory bulb, hippocampus, and hypothalamus (Supplementary Fig. 2). Coimmunostaining with either of two different anti-Glut4 antibodies and GFP in the hypothalamus of *GLUT4-Cre* × *Rosa26-Gfp* mice showed that >90% of GFP-positive cells (Fig. 1*A*–*D*) were also Glut4-positive (Fig. 1*E* and *F*), demonstrating that the transgene recapitulates faithfully the expression of the endogenous gene. To characterize Glut4-positive cells, we performed coimmunostaining with GFP and either the neuronal marker HuC/D or the glial marker Gfap throughout the CNS. The former, but not the latter, colocalized with Glut4 (Fig. 2). These data indicate that *GLUT4-Cre* induces recombination in a subset of neurons characterized by expression of Glut4 protein. We obtained similar data in the CNS of line 535 (data not shown).

Generation of GIRKO mice. To generate a model of insulin resistance in Glut4-cre–expressing tissues, we intercrossed transgenic line 546 with $Insr^{flox/flox}$ mice (7). The resulting $Insr^{flox/flox,GLUT4\text{-}cre}$ mice (Glut4-cre–driven InsR knockout, or GIRKO) showed InsR ablation in skeletal muscle, WAT, and BAT. A measurable decrease of InsR also could be detected in the hippocampus and mediobasal hypothalamus, but not in the cortex and cerebellum (Fig. 3*A* and Supplementary Fig. 5), consistent with the fact that most cells in the former two sites are Glut4-positive, whereas ~10% in the latter two sites are Glut4-positive (Supplementary Fig. 2). Accordingly, insulin-stimulated Akt phosphorylation was absent in skeletal muscle, including soleus and gastrocnemius, WAT (subcutaneous and epididymal), and BAT, whereas it was preserved in liver of GIRKO mice (Fig. 3*B*). We obtained identical results when we measured phospho-GSK-3 levels in response to insulin, indicating that Akt activity is impaired (Supplementary Fig. 3).

GIRKO mice develop insulin-resistant diabetes. GIRKO mice were born in the expected Mendelian ratios and showed no gross abnormality. A subset in both sexes developed hyperglycemia in the fed state (Fig. 4*A* and *B*) and hyperinsulinemia in the fed and fasted states (Supplementary Table 1, Fig. 4*C*). The prevalence of diabetes (defined as glycemia > mean + 2 SD) increased from 20% at 5 weeks to 25% at 12 weeks and 46% at 24 weeks of age in male mice, and hovered at approximately 10% in 5- to 12-week-old female mice. Intraperitoneal glucose tolerance and insulin tolerance tests in 12- to 13-week-old mice revealed modest glucose intolerance in male GIRKO mice and insulin resistance in female GIRKO mice, respectively (Supplementary Fig. 4).

Glucose clamps. To probe tissue-specific glucose metabolism and insulin sensitivity, we performed euglycemic-hyperinsulinemic clamps on 13- to 15-week-old nondiabetic male GIRKO and control littermates. Under basal conditions, blood glucose was slightly higher in GIRKO mice than in controls (119 vs. 87 mg/dL) (Fig. 5*A*). During the hyperinsulinemic phase of the clamp, we infused insulin to yield a similar increase in plasma insulin between the two groups (Supplementary Table 2) and achieved similar blood glucose levels at steady state. The rate of glucose infusion required to maintain euglycemia was decreased by 52% in GIRKO mice (Fig. 5*B*), consistent with impaired glucose disposal. Basal hepatic glucose production (HGP) was increased by 32% in GIRKO mice (Fig. 5*C*), and hyperinsulinemia was unable to suppress it (Fig. 5*D* and *E*), indicating marked hepatic insulin resistance. Moreover, the rate of glucose disappearance was reduced by 28% and glycolysis by 33% in GIRKO mice compared with

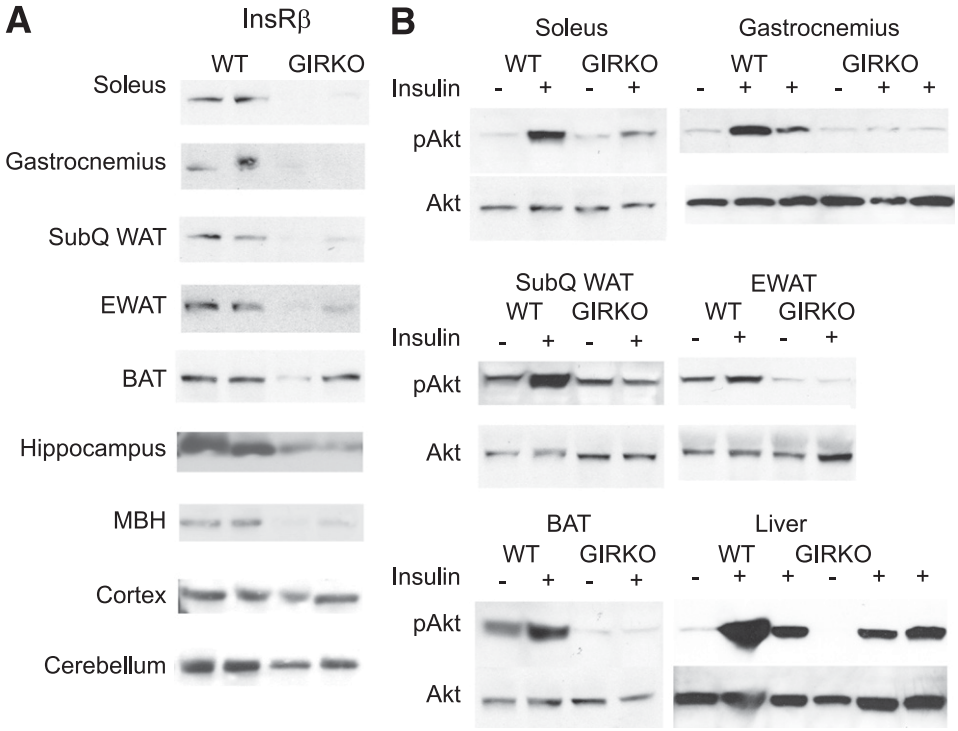

FIG. 3. Insulin signaling in GIRKO mice. *A*: Western blot analysis of InsR expression. Loading controls are shown in Supplementary Fig. 5. *B*: Insulin-dependent Akt phosphorylation in 12- to 14-week-old male normoglycemic GIRKO mice and control littermates (wild-type [WT]) after inferior vena cava injection of insulin or saline. Images shown are representative of four independent experiments.

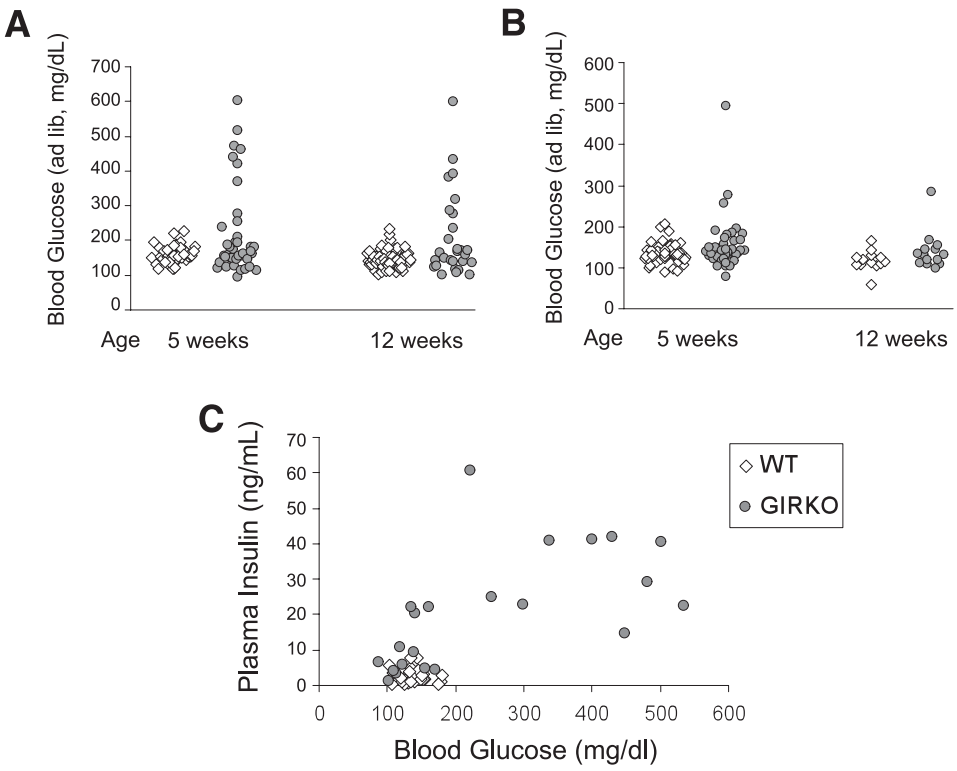

FIG. 4. Insulin and glucose levels. Scatter plots of blood glucose values in ad libitum (ad lib)-fed male (*A*) and female (*B*) WT and GIRKO littermates at 5 and 12 weeks of age. *C*: Scatter plot of blood glucose vs. serum insulin levels in ad libitum-fed 12-week-old male mice.

controls (Fig. 5*F* and *G*), whereas glycogen synthesis trended downward (Fig. 5*H*). Consistent with impaired insulin-dependent glucose uptake, 2-deoxy-glucose incorporation in gastrocnemius muscle was reduced by 34% in GIRKO mice (Fig. 5*I*). In contrast, 2-deoxy-glucose uptake in the cerebral cortex was not significantly altered (Fig. 5*J*), consistent with the insulin-independent mode of this process (mediated by Glut1 and Glut3) (22).

Given that hepatic insulin signaling (Fig. 3) and expression of genes encoding gluconeogenic enzymes are normal in GIRKO mice (data not shown), the increase of HGP is likely secondary to changes in humoral/neural factors or increased gluconeogenic precursors, such as FFA. Fasting FFA showed a nonsignificant decrease in GIRKO mice. Clamp hyperinsulinemia suppressed FFA by 43% in controls, but had no effect in GIRKO mice, consistent with reduced sensitivity of adipose tissue to insulin's antilipolytic actions (Supplementary Table 2). Fasting plasma glucagon and β-hydroxyl butyrate levels were similar between the two groups of mice (Supplementary Table 1), indicating that glucagon tone and fatty acid oxidation are normal in GIRKO mice. Hepatic triglyceride and glycogen content tended to be increased in overnight-fasted GIRKO mice compared with wild-type mice, but these changes did not reach statistical significance (Supplementary Table 1). The data suggest that failure to suppress FFA contributes to the increased HGP observed in hyperinsulinemic conditions, but cannot explain the increased basal HGP.

Morphologic analysis of BAT of 6-month-old GIRKO mice showed increased lipid droplet size and striking disruption of the multilocular structure that were more pronounced in diabetic GIRKO mice (Fig. 6*A*). Epididymal WAT of diabetic and nondiabetic GIRKO mice had a heterogeneous appearance compared with controls (Fig. 6*B*), reminiscent of the phenotype of fat-specific InsR knockouts (8). We also examined hepatic lipid and glycogen content by Oil red O and periodic acid-Schiff staining, respectively, and found hepatosteatosis and glycogen depletion only in diabetic GIRKO mice, whereas livers of nondiabetic GIRKO mice appeared normal (Fig. 6*C* and *D*).

β-Cell compensation and failure in GIRKO mice. We examined pancreatic islet morphology in 12-week-old male animals. Euglycemic GIRKO mice showed β-cell hyperplasia but maintained normal islet architecture (Fig. 7*A* and *B*). In contrast, diabetic GIRKO mice showed a leopard patterned loss of insulin immunoreactivity (Fig. 7*C*) (31), accompanied by loss of Pdx1 immunoreactivity (Fig. 7*D* and *E*), ectopic α-cells in the islet core (Fig. 7*F–H*), and loss of membrane localization of Glut2 (Fig. 7*J* and *K*).

Energy homeostasis in GIRKO mice. To determine whether InsR ablation in Glut4-expressing tissues affected energy homeostasis, we assessed respiratory exchanges by indirect calorimetry, coupled with food intake and activity determinations. GIRKO mice had normal body weight as weanlings, but showed persistent growth retardation thereafter, and weight of 16-week-old male mice was reduced by 19% compared with controls (Fig. 8*A*). The reduction in body weight affected equally lean and fat mass and was associated with normal plasma leptin levels (Supplementary Table 1). Diabetic GIRKO had significantly lower body weights than control or nondiabetic GIRKO mice (data not shown).

Body weight in the cohort that underwent indirect calorimetry determinations showed the same distribution as in the population as a whole (Fig. 8*B*). Daily food intake was similar between controls and nondiabetic GIRKO mice (Fig. 8*C*), but the latter displayed altered circadian feeding patterns, consuming only 26% of total food during

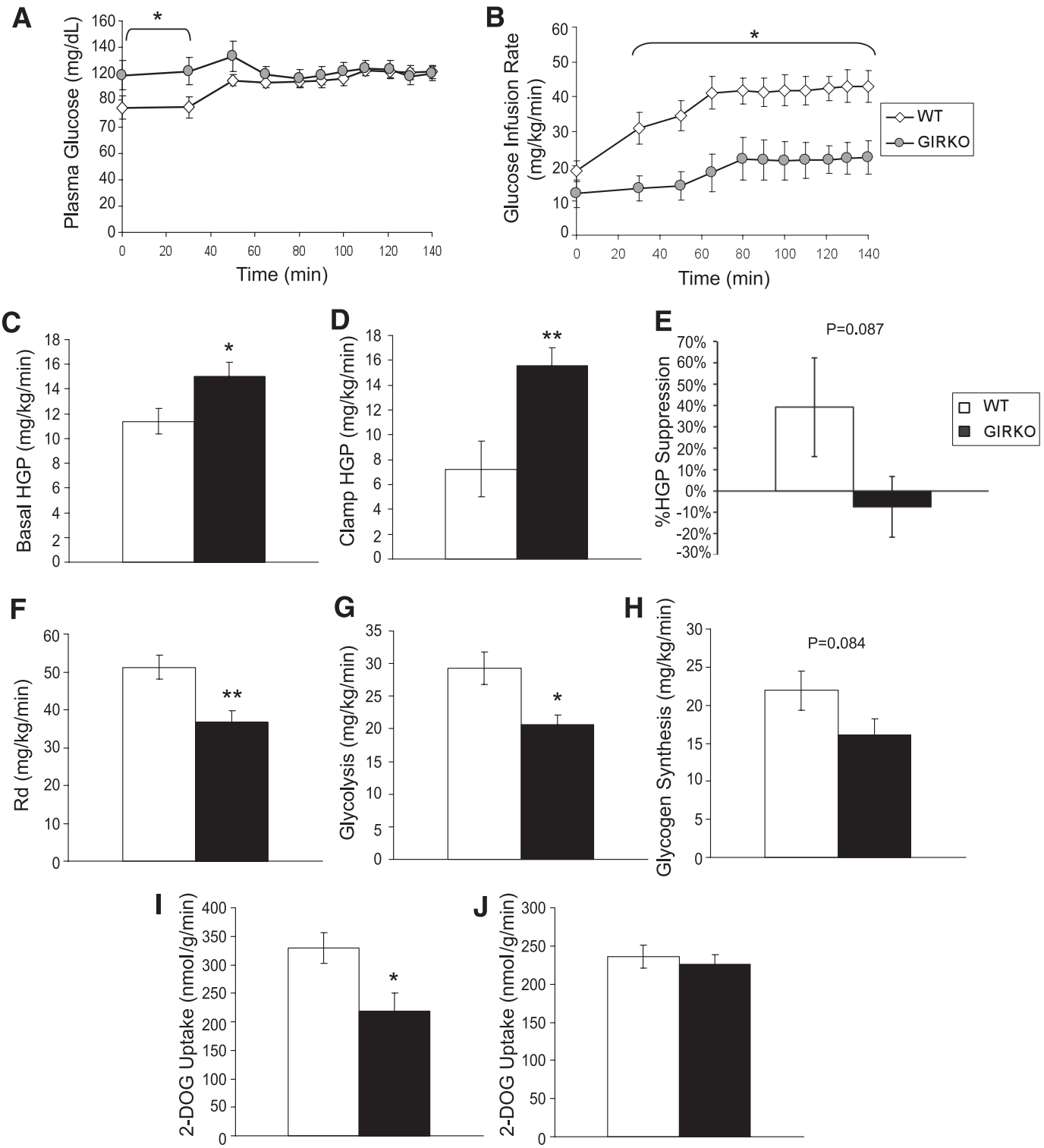

FIG. 5. Hyperinsulinemic euglycemic clamps. *A*: Blood glucose of 13- to 15-week-old male WT and GIRKO mice during the clamp studies. *B*: Glucose infusion rate during the clamp. HGP during basal (*C*) and hyperinsulinemic (*D*) periods of the clamp. *E*: Suppression of HGP by hyperinsulinemia. Rate of glucose disappearance (*F*), glycolysis (*G*), and glycogen synthesis (*H*) during the clamp. Uptake of 2-deoxyglucose (2-DOG) during the last 10 min of the clamp in gastrocnemius (*I*) and cerebral cortex (*J*). Data are mean ± SEM. n = 9–10. *$P < 0.05$, **$P < 0.01$ vs. WT.

the light phase compared with 34% in control mice (Fig. 8*D*). In addition, oxygen consumption and locomotion were largely unperturbed in nondiabetic GIRKO mice (Fig. 8*E*–*G*). In diabetic GIRKO mice, food intake was increased when normalized by body weight (Fig. 8*C*), but total intake per animal was similar to that of control and nondiabetic GIRKO mice (Fig. 8*D*). In addition, although oxygen consumption in diabetic GIRKO mice showed an increase when normalized by body weight (Fig. 8*E*), total energy expenditure per animal tended to decrease (Fig. 8*F*),

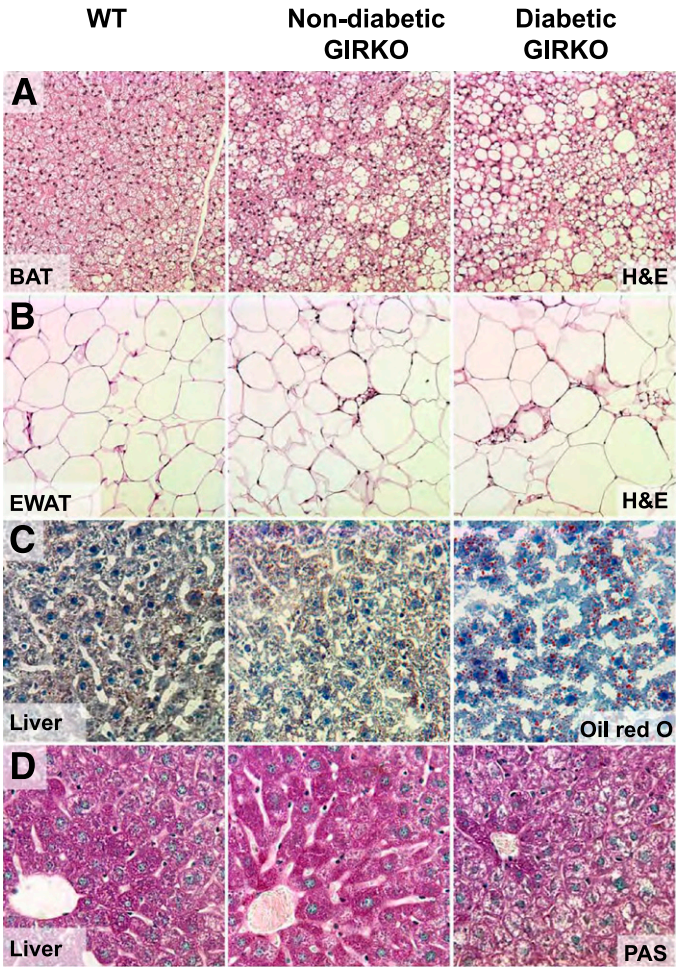

FIG. 6. Adipose and liver histology. Hematoxylin–eosin stain of BAT (*A*) and epididymal WAT (*B*), and Oil red O stain (*C*) and periodic acid-Schiff stain (*D*) of liver in 6-month-old male mice killed in the ad libitum-fed state. *Left*: Control mice (WT). *Middle*: Nondiabetic GIRKO. *Right*: Diabetic GIRKO mice. (A high-quality digital representation of this figure is available in the online issue.)

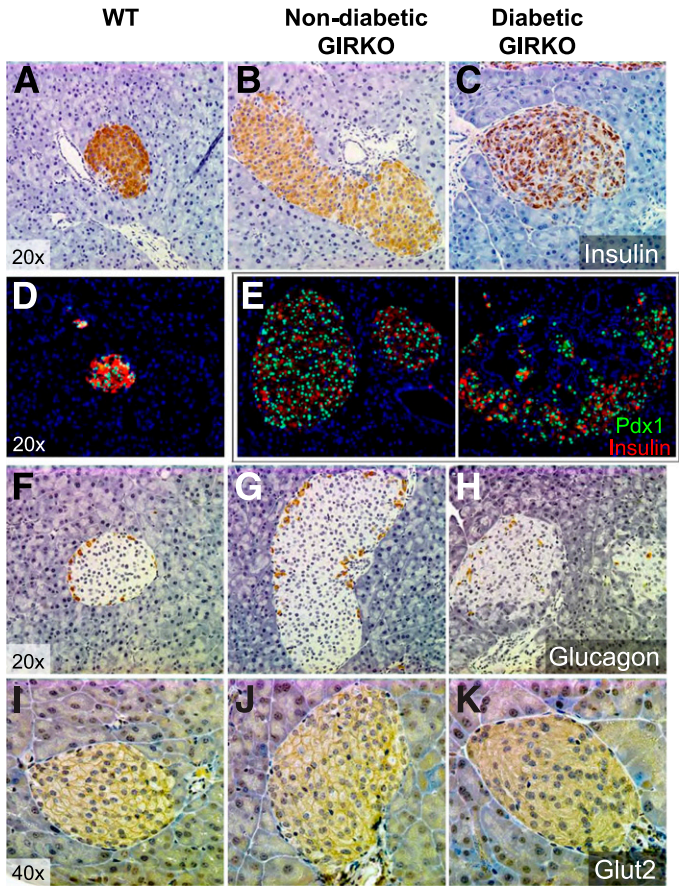

FIG. 7. Pancreatic islet morphology. Immunohistochemistry with antibodies against insulin (brown) (*A–C*), Pdx1 (green) and insulin (red) (*D*, *E*), glucagon (brown) (*F–H*), and Glut2 (brown) (*I–K*). Cell nuclei are visualized by Hoechst stain (blue). *Left*: Control mice (WT). *Middle*: Nondiabetic GIRKO. *Right*: Diabetic GIRKO mice. Representative images are shown. (A high-quality digital representation of this figure is available in the online issue.)

consistent with reduced lean body mass and unchanged locomotion (Fig. 8*G*). Furthermore, respiratory exchange ratio and carbohydrate use in diabetic GIRKO mice failed to show circadian variations, with no discernible increase after food ingestion during the dark phase (Fig. 8*H* and *I*). Taken together, these data indicate that InsR ablation in Glut4-expressing neurons does not alter energy intake or expenditure, but may affect circadian feeding patterns. The changes seen in hyperglycemic GIRKO mice, including metabolic substrate inflexibility, altered rhythmicity in substrate use, relative hyperphagia, and weight loss from impaired nutrient storage, are presumably secondary to diabetes.

DISCUSSION

The key finding of this study is that selective impairment of insulin action in Glut4-expressing tissues, in the absence of primary changes to liver and pancreatic β-cell function, results in a murine model of T2D that faithfully recapitulates the human disease. Further, the study identifies a heretofore ill-characterized entity that we propose to name "Glut4 neuron," as a site of insulin action. Our findings provide a solution to the conundrum on the site of onset of insulin resistance, expand our understanding of the neuroanatomy and cellular physiology of insulin action in the CNS, and integrate the latter into the broader picture of diabetes pathogenesis.

An integrated view of diabetes pathophysiology. Identifying the sites of onset of insulin resistance is necessary if we are to develop a rational approach to treating this condition—a cornerstone of diabetes therapy (32). Single InsR knockouts in individual tissues have been more notable for what they failed to cause than for what they did cause (33), as was the combined InsR ablation in muscle/fat (6). Why is the InsR knockout in Glut4-expressing tissues able to cause diabetes? Probably because, in addition to the impairment of peripheral glucose disposal caused by InsR knockout in muscle and fat, and unlike other models of impaired InsR signaling in muscle (34) or fat (8), GIRKO mice develop profound hepatic insulin resistance and β-cell dysfunction. We favor the interpretation that the former is due to impaired InsR signaling in Glut4 neurons (16,35,36), with a possible contributory role of other factors, such as FFA. Given that most hypothalamic neurons appear to be Glut4-positive, it is likely that InsR signaling in these neurons contributes to insulin's demonstrated ability to control HGP via the CNS (16,35,36). Our data do not imply that InsR ablation in Glut4 neurons is the sole cause of diabetes. Rather, they suggest that the combination of muscle, fat,

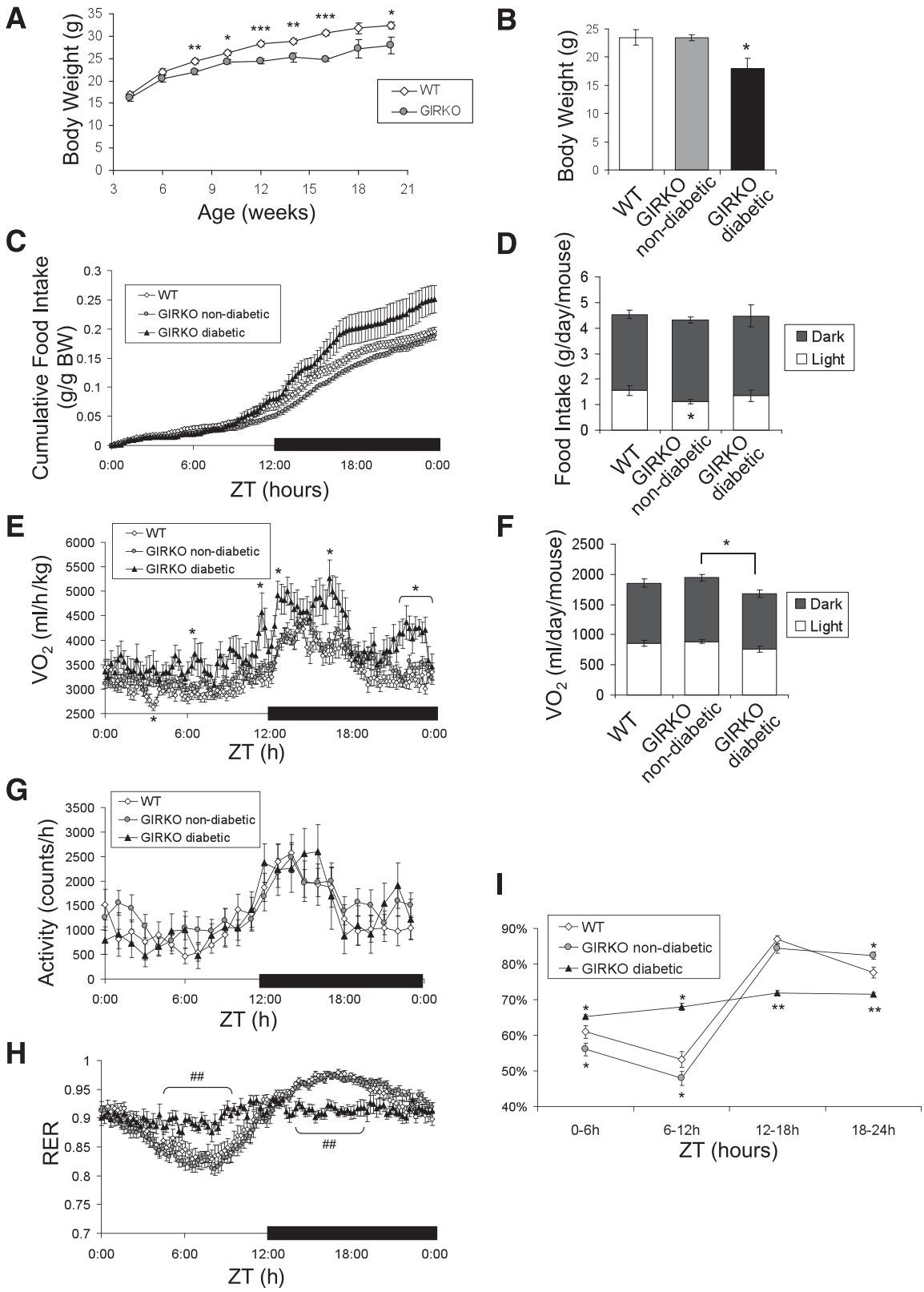

FIG. 8. Energy homeostasis. *A*: Body weight of male WT and GIRKO mice. *B*: Body weight of 9-week-old male WT, nondiabetic GIRKO, and diabetic GIRKO mice used for indirect calorimetry study. *C*: Cumulative food intake measured during calorimetry study normalized by total body weight. *D*: Food intake per animal per day during the light and dark phases. Oxygen consumption normalized by body weight (*E*) or per animal (*F*). *G*: Locomotor activity. *H*: Respiratory exchange ratio (RER). *I*: Substrate use was estimated on the basis of the assumptions that *1*) protein catabolism is negligible and *2*) RER of carbohydrate catabolism is 1 and RER of fat catabolism is 0.7. Percentage of carbohydrate use is calculated with the formula %Carbohydrate = (RER − 0.7) / 0.3. Data are mean ± SEM. *n* = 7 (WT), 10 (nondiabetic GIRKO), and 3 (diabetic GIRKO). Mice were habituated 24–36 h, and measurements were taken for 4–5 consecutive days. **P* < 0.05, ***P* < 0.01, ****P* < 0.01 between groups. ##*P* < 0.01 vs. WT and nondiabetic GIRKO.

and CNS insulin resistance underlies the transition from euglycemic insulin resistance to diabetes.

It is also intriguing that InsR ablation in Glut4 neurons did not affect total energy intake or expenditure, but rather shifted circadian patterns of feeding and substrate use. A large body of literature indicates that disruption of the circadian clock in the CNS or peripheral tissues can lead to insulin resistance, defects in insulin secretion, and other manifestations of the metabolic syndrome (37,38). Further studies will be necessary to determine whether alterations in the circadian rhythm contribute to the cause of diabetes in GIRKO mice.

Profound abnormalities of β-cell mass represent another distinguishing feature of GIRKO mice from other models of peripheral insulin resistance due to alterations of InsR signaling (25,39). We speculate that the β-cell abnormality is also secondary to impaired CNS control of endocrine pancreatic function. But we cannot rule that other sites of InsR ablation in GIRKO mice (e.g., vessel wall, exocrine pancreas, or other as yet undiscovered locations) contribute to this process. Nonetheless, the combined presence of cell-autonomous mechanisms of insulin resistance (in muscle/fat) and cell-nonautonomous mechanisms (in liver and β-cell) in GIRKO mice indicates that Glut4-expressing tissues play a direct role as metabolic targets for nutrient disposal and storage, and a "sensing" role through which they are able to affect liver and endocrine pancreatic function.

Glut4 neurons and Glut4 function in the CNS. The presence of Glut4 in the CNS has long been a puzzle, partly because of the presence of additional glucose transporters, partly to lingering controversies as to its precise localization (17,20,21,29,30,40–43), and partly to limited ability to probe its function in this organ. Our study conclusively demonstrates that neurons, not glia, are the site of Glut4 expression. Their distribution and morphology bespeak heterogeneous functions, potentially including locomotor and learning behaviors. In the hypothalamus, Glut4 neurons could reasonably partake in glucose sensing, counterregulation, and food intake (44). Their functions are likely to extend beyond the functions of Glut4 *itself*. But it is interesting that Glut4 ablation in the CNS impairs glucose sensing and glucose tolerance (44). Brain glucose sensing is important for counterregulation in response to hypoglycemia and is altered by obesity and antecedent hypoglycemia (45). Although most, if not all, glucose-sensing neurons express both InsR and Glut4 (46), the general view is that, under euglycemic conditions, glucose sensing occurs independently of insulin, probably through Glut3 and glucokinase (45). It is possible, however, that InsR signaling leads to Glut4 translocation, thus increasing local glucose concentrations at discrete sites within the cell body or neuronal processes to levels that allow for glucokinase activation, ATP generation, and closure of K_{ATP} channels (47), with increased firing of glucose-excited neurons (48).

Insulin resistance remains a large unmet medical need, and clinically effective agents that partly restore insulin sensitivity remain limited to metformin and pioglitazone. Because insulin signaling is pleiotropic and entails different biological outcomes in different cell types, the rational design of insulin sensitizers must rely on detailed knowledge of the cellular sites and biochemical processes of insulin resistance. GIRKO mice should prove widely useful as a monogenic model of insulin-resistant diabetes, devoid of the confounders generally associated with other commonly used models.

ACKNOWLEDGMENTS

This research was supported by the Berrie Fellowship Award (to H.V.L.); National Institutes of Health Grants DK-58282, DK-57539 (to D.A.), and DK-40936 (to G.I.S.); the Columbia University Diabetes and Endocrinology Research Center (DK-63608); and the Mouse Metabolic Phenotyping Center (U24 DK-076169).

No potential conflicts of interest relevant to this article were reported.

H.V.L. designed and conducted experiments, analyzed data, and wrote the article; H.R. designed and conducted experiments, analyzed data, and wrote the article; V.T.S. and H.-Y.L. conducted glucose clamp experiments; T.Y.L. conducted experiments; G.I.S. designed experiments, analyzed data, and wrote the article; and D.A. designed experiments, analyzed data, and wrote the article.

The authors thank C.R. Kahn (Joslin Diabetes Center) for the gift of the floxed *InsR* mice, K. Aizawa, A. Flete, Y. Dam, V. Lin, and Q. Xu (Columbia University) for technical assistance, and members of the Accili laboratory for helpful discussions and critical reading of the article.

REFERENCES

1. Accili D. Lilly lecture 2003: the struggle for mastery in insulin action: from triumvirate to republic. Diabetes 2004;53:1633–1642
2. Bouché C, Serdy S, Kahn CR, Goldfine AB. The cellular fate of glucose and its relevance in type 2 diabetes. Endocr Rev 2004;25:807–830
3. Graham TE, Kahn BB. Tissue-specific alterations of glucose transport and molecular mechanisms of intertissue communication in obesity and type 2 diabetes. Horm Metab Res 2007;39:717–721
4. Petersen KF, Dufour S, Savage DB, et al. The role of skeletal muscle insulin resistance in the pathogenesis of the metabolic syndrome. Proc Natl Acad Sci U S A 2007;104:12587–12594
5. Shoelson SE, Lee J, Goldfine AB. Inflammation and insulin resistance. J Clin Invest 2006;116:1793–1801
6. Lauro D, Kido Y, Castle AL, et al. Impaired glucose tolerance in mice with a targeted impairment of insulin action in muscle and adipose tissue. Nat Genet 1998;20:294–298
7. Brüning JC, Michael MD, Winnay JN, et al. A muscle-specific insulin receptor knockout exhibits features of the metabolic syndrome of NIDDM without altering glucose tolerance. Mol Cell 1998;2:559–569
8. Blüher M, Michael MD, Peroni OD, et al. Adipose tissue selective insulin receptor knockout protects against obesity and obesity-related glucose intolerance. Dev Cell 2002;3:25–38
9. Kotani K, Peroni OD, Minokoshi Y, Boss O, Kahn BB. GLUT4 glucose transporter deficiency increases hepatic lipid production and peripheral lipid utilization. J Clin Invest 2004;114:1666–1675
10. Nakae J, Biggs WH 3rd, Kitamura T, et al. Regulation of insulin action and pancreatic beta-cell function by mutated alleles of the gene encoding forkhead transcription factor Foxo1. Nat Genet 2002;32:245–253
11. Okada T, Liew CW, Hu J, et al. Insulin receptors in beta-cells are critical for islet compensatory growth response to insulin resistance. Proc Natl Acad Sci U S A 2007;104:8977–8982
12. Kahn BB, Rossetti L. Type 2 diabetes—who is conducting the orchestra? Nat Genet 1998;20:223–225
13. Schwartz MW, Porte D Jr. Diabetes, obesity, and the brain. Science 2005;307:375–379
14. Brüning JC, Gautam D, Burks DJ, et al. Role of brain insulin receptor in control of body weight and reproduction. Science 2000;289:2122–2125
15. Okamoto H, Nakae J, Kitamura T, Park BC, Dragatsis I, Accili D. Transgenic rescue of insulin receptor-deficient mice. J Clin Invest 2004;114:214–223
16. Lin HV, Plum L, Ono H, et al. Divergent regulation of energy expenditure and hepatic glucose production by insulin receptor in agouti-related protein and POMC neurons. Diabetes 2010;59:337–346
17. Vannucci SJ, Koehler-Stec EM, Li K, Reynolds TH, Clark R, Simpson IA. GLUT4 glucose transporter expression in rodent brain: effect of diabetes. Brain Res 1998;797:1–11
18. Cheng CM, Reinhardt RR, Lee WH, Joncas G, Patel SC, Bondy CA. Insulin-like growth factor 1 regulates developing brain glucose metabolism. Proc Natl Acad Sci U S A 2000;97:10236–10241
19. Komori T, Morikawa Y, Tamura S, Doi A, Nanjo K, Senba E. Subcellular localization of glucose transporter 4 in the hypothalamic arcuate nucleus of ob/ob mice under basal conditions. Brain Res 2005;1049:34–42

20. Bakirtzi K, Belfort G, Lopez-Coviella I, et al. Cerebellar neurons possess a vesicular compartment structurally and functionally similar to Glut4-storage vesicles from peripheral insulin-sensitive tissues. J Neurosci 2009; 29:5193–5201
21. Apelt J, Mehlhorn G, Schliebs R. Insulin-sensitive GLUT4 glucose transporters are colocalized with GLUT3-expressing cells and demonstrate a chemically distinct neuron-specific localization in rat brain. J Neurosci Res 1999;57:693–705
22. Vannucci SJ, Clark RR, Koehler-Stec E, et al. Glucose transporter expression in brain: relationship to cerebral glucose utilization. Dev Neurosci 1998;20:369–379
23. Olson AL, Liu ML, Moye-Rowley WS, Buse JB, Bell GI, Pessin JE. Hormonal/metabolic regulation of the human GLUT4/muscle-fat facilitative glucose transporter gene in transgenic mice. J Biol Chem 1993;268:9839–9846
24. Matsumoto M, Pocai A, Rossetti L, Depinho RA, Accili D. Impaired regulation of hepatic glucose production in mice lacking the forkhead transcription factor Foxo1 in liver. Cell Metab 2007;6:208–216
25. Kido Y, Burks DJ, Withers D, et al. Tissue-specific insulin resistance in mice with mutations in the insulin receptor, IRS-1, and IRS-2. J Clin Invest 2000;105:199–205
26. Plum L, Lin HV, Dutia R, et al. The obesity susceptibility gene Cpe links FoxO1 signaling in hypothalamic pro-opiomelanocortin neurons with regulation of food intake. Nat Med 2009;15:1195–1201
27. Kitamura YI, Kitamura T, Kruse JP, et al. FoxO1 protects against pancreatic beta cell failure through NeuroD and MafA induction. Cell Metab 2005; 2:153–163
28. Xuan S, Kitamura T, Nakae J, et al. Defective insulin secretion in pancreatic beta cells lacking type 1 IGF receptor. J Clin Invest 2002;110:1011–1019
29. El Messari S, Leloup C, Quignon M, Brisorgueil MJ, Penicaud L, Arluison M. Immunocytochemical localization of the insulin-responsive glucose transporter 4 (Glut4) in the rat central nervous system. J Comp Neurol 1998;399: 492–512
30. Sankar R, Thamotharan S, Shin D, Moley KH, Devaskar SU. Insulin-responsive glucose transporters-GLUT8 and GLUT4 are expressed in the developing mammalian brain. Brain Res Mol Brain Res 2002;107:157–165
31. Kitamura T, Nakae J, Kitamura Y, et al. The forkhead transcription factor Foxo1 links insulin signaling to Pdx1 regulation of pancreatic beta cell growth. J Clin Invest 2002;110:1839–1847
32. Kahn SE, Haffner SM, Heise MA, et al.; ADOPT Study Group. Glycemic durability of rosiglitazone, metformin, or glyburide monotherapy. N Engl J Med 2006;355:2427–2443
33. Kitamura T, Kahn CR, Accili D. Insulin receptor knockout mice. Annu Rev Physiol 2003;65:313–332
34. Kim JK, Michael MD, Previs SF, et al. Redistribution of substrates to adipose tissue promotes obesity in mice with selective insulin resistance in muscle. J Clin Invest 2000;105:1791–1797
35. Könner AC, Janoschek R, Plum L, et al. Insulin action in AgRP-expressing neurons is required for suppression of hepatic glucose production. Cell Metab 2007;5:438–449
36. Obici S, Zhang BB, Karkanias G, Rossetti L. Hypothalamic insulin signaling is required for inhibition of glucose production. Nat Med 2002;8:1376–1382
37. Turek FW, Joshu C, Kohsaka A, et al. Obesity and metabolic syndrome in circadian Clock mutant mice. Science 2005;308:1043–1045
38. Kohsaka A, Laposky AD, Ramsey KM, et al. High-fat diet disrupts behavioral and molecular circadian rhythms in mice. Cell Metab 2007;6:414–421
39. Brüning JC, Winnay J, Bonner-Weir S, Taylor SI, Accili D, Kahn CR. Development of a novel polygenic model of NIDDM in mice heterozygous for IR and IRS-1 null alleles. Cell 1997;88:561–572
40. McEwen BS, Reagan LP. Glucose transporter expression in the central nervous system: relationship to synaptic function. Eur J Pharmacol 2004; 490:13–24
41. Vannucci SJ, Maher F, Simpson IA. Glucose transporter proteins in brain: delivery of glucose to neurons and glia. Glia 1997;21:2–21
42. Maher F, Vannucci SJ, Simpson IA. Glucose transporter proteins in brain. FASEB J 1994;8:1003–1011
43. Maher F, Simpson IA, Vannucci SJ. Alterations in brain glucose transporter proteins, GLUT1 and GLUT3, in streptozotocin diabetic rats. Adv Exp Med Biol 1993;331:9–12
44. Puente EC, Daphna-Iken D, Bree AJ, et al. Impaired glucose tolerance and counterregulatory response to hypoglycemia in brain glucose transporter 4 (GLUT4) knockout mice. Diabetes 2009;58(Suppl. 1):49
45. Levin BE, Routh VH, Kang L, Sanders NM, Dunn-Meynell AA. Neuronal glucosensing: what do we know after 50 years? Diabetes 2004;53:2521–2528
46. Kang L, Routh VH, Kuzhikandathil EV, Gaspers LD, Levin BE. Physiological and molecular characteristics of rat hypothalamic ventromedial nucleus glucosensing neurons. Diabetes 2004;53:549–559
47. Miki T, Liss B, Minami K, et al. ATP-sensitive K+ channels in the hypothalamus are essential for the maintenance of glucose homeostasis. Nat Neurosci 2001;4:507–512
48. Wang R, Liu X, Hentges ST, et al. The regulation of glucose-excited neurons in the hypothalamic arcuate nucleus by glucose and feeding-relevant peptides. Diabetes 2004;53:1959–1965